CHEMISTRY OF MATERIALS

Article

pubs.acs.org/cm

Augmenting n-Type Performance of Ambipolar Top-Contact Organic Thin-Film Transistors by Self-Generated Interlayers

Tanmoy Sarkar,[†] Jane Vinokur,[†] Basel Shamieh,[†] Victoria Savikhin,[#,‡] Michael F. Toney,[#] and Gitti L. Frey*[,†]

[†]Department of Materials Science and Engineering, Technion—Israel Institute of Technology, Haifa 32000, Israel

[#]SLAC National Accelerator Laboratory, 2575 Sand Hill Road, Building 137, Menlo Park, California 94025, United States

[‡]Electrical Engineering Department, Stanford University, 350 Serra Mall, Stanford, California 94305, United States

Supporting Information

ABSTRACT: We report n-type performance enhancement of an ambipolar donor−acceptor (D−A) polymer by suppressing its p-type behavior using a simple and versatile methodology of interlayer processing in top-contact organic field-effect transistors. In this approach, a judiciously selected interlayer material, polyethylene glycol (PEG), is codeposited as an additive with the semiconducting polymer DPP-T-TT active layer. During top-contact aluminum deposition, the PEG molecules migrate from within the bulk film to the organic/Al interface because of additive−metal interactions. The formation of the PEG interlayer was confirmed by X-ray photoelectron spectroscopy and its effect on the polymeric-interfacial microstructure was studied using angle-dependent grazing-incidence wide-angle X-ray scattering. We find that the PEG interlayer has two significant contributions to the n-type characteristics of the device: it suppresses hole injection while improving electron injection by tuning the effective work-function, and it enhances the order and crystallinity of the polymer at the interface effectively enhancing charge mobility.

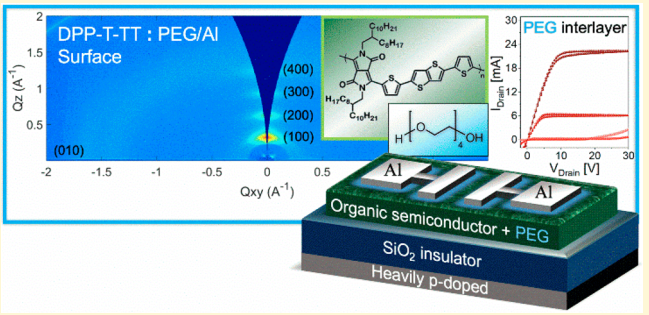

INTRODUCTION

Solution-processed organic field-effect transistors (OFETs) are essential building blocks for a variety of electronic devices such as radio frequency identification (RFID) tags, flexible displays, memory devices, medical sensors, and so on.[1−5] This drives intense efforts in the design and synthesis of π-conjugated polymers consisting of alternating electron donor (D) and acceptor (A) units. The ground state of such polymers has partial charge-transfer character endowing them with ambipolar semiconducting properties. The relative strength of the donor or acceptor components determines the type of majority charge carrier in the polymer.[6,7] High-mobility D−A polymers are predominantly p-type with holes as majority carriers. For example, polar diketopyrrolo-pyrrole (DPP)-based D−A polymers, with either side chain engineering[8] or ammonium salt incorporation,[9] showed p-type mobility of 12 cm^2 V^{-1} s^{-1} and 13.7 cm^2 V^{-1} s^{-1}, respectively. However, the lack of acceptor building blocks with efficient electron-transport capabilities limits the availability of high-mobility n-type organic semiconductors.[7,10] Yet, both p-channel and n-channel are required for complementary metal oxide semiconductor (CMOS)-like logic circuits using organic thin film transistors (OFETs). Therefore, augmenting the n-type performance of ambipolar D−A polymers by suppressing its p-type behavior is a promising route for n-channel polymer-based OFETs. For example, Sun et al. used poly ethylenimine (PEI) as a hole-trapping dopant in an ambipolar D−A semiconducting polymer effectively converting it into a high-performance unipolar n-type film for OFETs.[11]

The n-type performance of D−A ambipolar polymers is also limited by contact resistance that generally has two contributions in series: the Schottky barrier and the bulk-access resistance. In most cases, bulk-access resistance is significantly lower than the Schottky barrier and hence ignored.[12,13] The Schottky barrier is imposed by the energy difference between the shallow lowest unoccupied molecular orbital (LUMO) of the D−A polymer and the work function of the contact. Accordingly, alignment of the metal electrode work function to the LUMO level of the polymer is a practical approach to enhance electron injection/extraction and hence n-type device performance. Cheng et al. reported that a self-assembled monolayer (SAM) of thiol-capped molecules positioned at the organic/silver interface modifies the effective work function (EWF) and enhances n-type OFET performance.[14,15] Furthermore, circumstantial evidence showed that

Special Issue: Jean-Luc Bredas Festschrift

Received: May 7, 2019
Revised: June 20, 2019
Published: June 21, 2019

DOI: 10.1021/acs.chemmater.9b01787
Chem. Mater. XXXX, XXX, XXX−XXX

the SAM could also direct an interfacial microstructure that is favorable for electron injection. However, SAM deposition generally requires distinct processing steps that are often cost-effective and could considerably complicate device fabrication.[14,16,17]

Recently, we reported on tuning the EWF at metal/organic interfaces using self-generated interlayers and associated performance enhancement in top-contact OFETs, organic solar cells (OSCs), and organic light-emitting diodes (OLEDs).[18,19] In this methodology, molecules with moieties that have affinity to the electrode metal, for example, O−H to Al or S−H to Ag, are initially blended as additives in the semiconducting polymer film and spontaneously migrate to the polymer/metal interface during metal deposition. Additive migration stops once a complete interlayer, fully covering the metal contact, is formed and the driving force for migration is terminated. During the migration process, the bulk film is depleted of the additive molecules which are now situated at the polymer/metal interface.[19] Additive migration through the polymer to the top interface depends on the affinity of the additive molecules to the metal electrode compared to its affinity to the polymer host and/or the bottom substrate. Additive size, system temperature, and polymer crystallinity can also affect additive migration.[20−22] Using this method we recently demonstrated EWF modification of the polymer/metal interface in both p- and n-type OFETs, leading to significant reduction of contact resistance and improved performances.[18]

Here we show that the self-generated interlayer method can also be used to suppress p-type characteristics and augment n-type performance of ambipolar D−A semiconducting polymers in OFETs. We selected diketopyrrolopyrrolethieno[3,2-*b*]-thiophene D−A copolymer (DPP-T-TT) (Figure 1a) because

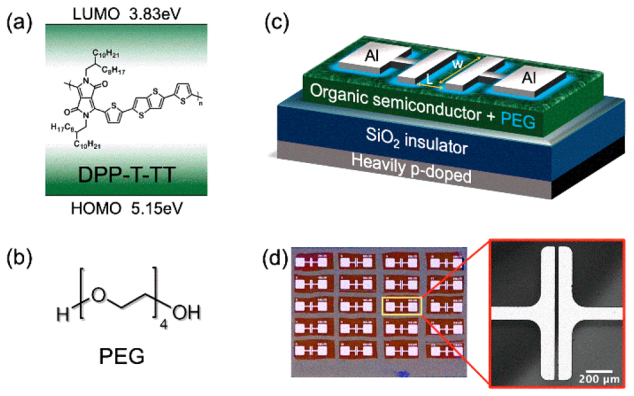

Figure 1. Chemical structures, device schematic and optical images of (a) semiconducting polymer DPP-T-TT, (b) PEG additive, (c) bottom-gate top-contact OFET, and (d) optical image of a substrate containing 20 devices with different channel lengths, L = 30, 40, 50, and 80 μm; and W = 1000 μm. Inset: microscopic image of a single OFET device (W/L = 1000/30).

it previously showed hole mobility approaching nearly 1 cm^2 V^{-1} s^{-1} in p-type OFETs but moderate n-type mobility even after high-temperature annealing (~320 °C). Notably, the factors limiting high n-type mobility in DPP-T-TT were not clearly understood.[23] In this study, we chose polyethylene glycol (PEG) as an additive to modify the EWF of the buried organic/aluminum (Al) interface because it was shown to induce a dipole moment at the organic/Al junction that reduces the energy barrier for charge injection.[24] Furthermore, PEG strongly interacts with Al and hence is expected to migrate to the DPP-T-TT/Al interface during Al deposition.[25,26] X-ray photoelectron spectroscopy (XPS) confirms that the additive enriches the DPP-T-TT/Al interface, and 2D grazing incidence wide-angle X-ray scattering (GIWAXS) reveals, for the first time, that the self-generated interlayer induces a high degree of polymer order, crystallinity, and orientation at the polymer/metal interface. Bottom-gate top-contact OFET device measurements and transfer line method (TLM) analysis show suppression of contact resistance with interlayer formation. The interfacial electronic structure (i.e., EWF modification) and materials microstructure (i.e., high degree of polymer order, imposed by the self-generated interlayer) lead to a significant reduction of contact resistance for electron injection/extraction, suppression of p-type character, and overall improvement of n-type device performances.

RESULTS AND DISCUSSION

The ambipolar D−A polymer DPP-T-TT has a HOMO level at 5.25 (±0.5) eV,[6,18,27] bandgap of 1.42 eV (see absorption spectra in Figure S1 of the Supporting Information), and accordingly a LUMO level at 3.83 (±0.5) eV (Figure 1a).[27] The work function of Al is ~4.15 eV, and therefore, when Al and DPP-T-TT are brought in contact, a high Schottky barrier ($\Delta\phi_b \approx 0.32$ eV) and wide image-charge potential develop at the DPP-T-TT/Al interface, effectively limiting electron injection.[28] Insertion of a monolayer or an ultrathin insulating layer at the organic semiconductor/metal interface is known to reduce the Schottky barrier.[18,29] We recently showed that PEG, which contains methane-hydroxyl end groups and polar O−C bonds in the backbone (Figure 1b), can reduce the EWF at polymer/Al electrode interfaces by modifying the interface dipole.[24] The surface energy of PEG oligomers (43 mJ m^{-2}) is higher than that of DPP-T-TT (~33.16 mJ m^{-2}), so PEG molecules are not expected to enrich the surface of the spun film.[30,31] However, following our previous report, we suggest that the affinity of the O−H end-groups to Al induces the self-segregation of PEG molecules to the polymer/Al interface during Al deposition.[19] To generate a PEG interlayer at the DPP-T-TT/Al interface in OFETs, we blended PEG molecules into the DPP-T-TT solution and collectively spun onto a thin film. XPS measurements of the DPP-T-TT:PEG/Air and DPP-T-TT:PEG/Al interfaces show no traces of PEG molecules at the film/air interface but do show the presence of PEG under the Al contact (Figure S2 of the Supporting Information). These spectra confirm the migration of PEG molecules toward the Al contact and the generation of a PEG interlayer at the DPP-T-TT/Al interface.

After confirming the presence of the PEG interlayer, we study its effect on contact selectively in DPP-T-TT OFETs bottom-gate top-contact devices. Figure 1c,d show the device architecture and optical image of a silicon substrate containing 20 devices with different channel lengths but similar channel width. The output and transfer characteristics of pristine DPP-T-TT OFETs are shown in panels a and d, respectively, of Figure 2 (black line). The calculated saturation electron mobility of pristine DPP-T-TT is 0.03 ± 0.015 cm^2 V^{-1} s^{-1} (using V_{th} = 16.1 V and equation S1 of the Supporting Information). Notably, the pristine DPP-T-TT device exhibits overall low drain current with a nonlinear S-shape current−voltage dependence at low source−drain voltages (Figure 2a

DOI: 10.1021/acs.chemmater.9b01787
Chem. Mater. XXXX, XXX, XXX−XXX

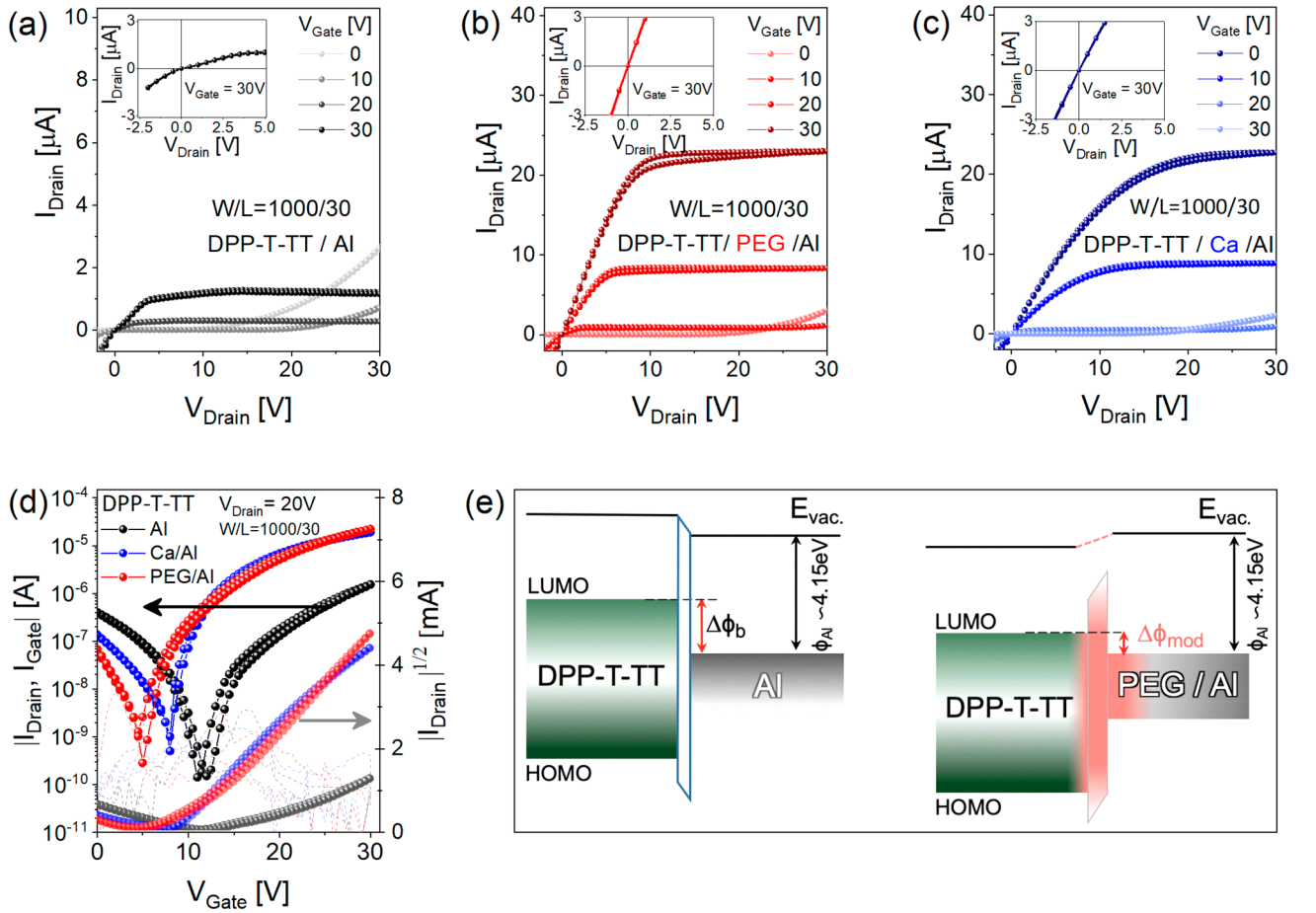

Figure 2. DPP-T-TT OFETs device performance with and without a PEG interlayer. Output characteristics of devices with 30 μm channel length and 1000 μm channel width at V_{Gate} = 0, 10, 20, and 30 V of (a) pristine, (b) with PEG interlayer, and (c) Ca/Al contact. Insets show the linear region (V_{Drain}: 2.5 to −5 V) output characteristics. (d) Transfer characteristics of the same devices. Dashed lines represent the gate currents (I_{Gate}) corresponding to each device. (e) Energy level diagram at DPP-T-TT/Al and DPP-T-TT/PEG/Al interface.

inset), indicative of high resistance to electron injection. This contact resistance is associated with a high Schottky barrier between the LUMO level of DPP-T-TT and the work function of Al, as schematically illustrated in Figure 2e (left panel). As a consequence of the low charge carrier density, the turn-on voltage of this device is remarkably high (11.5 V).[16]

Presence of the self-generated PEG interlayer at the DPP-T-TT/Al interface leads to an overall increase of the I_{Drain} by an order of magnitude, as shown in Figure 2b. In contrast to the pristine device, the drain current increases linearly at low drain-source voltage (Figure 2b inset) suggesting Ohmic electron injection through the contact. The calculated saturation electron mobility (with V_{th} = 10 V and equation S1 of the Supporting Information) is 0.23 ± 0.04 cm^2 V^{-1} s^{-1}, over an order of magnitude higher than that of the pristine device. This n-type mobility value is comparable with that reported for high-temperature-processed DPP-T-TT, despite the room-temperature processing of these devcies.[23] The transfer characteristics in Figure 2d show that the self-generated PEG interlayer leads to a substantial reduction of the turn-on voltage, from 11.5 to 5.2 V at V_{Drain} = 20 V, associated with a reduction of the barrier for electron injection and the consequent increase of electron density by 5.4 × 10^{11} cm^{-2} (estimated using the parallel capacitance model equation, as described in Figure S3 in the Supporting Information section).[16]

To corroborate the contribution of the PEG interlayer to contact selectivity and not to the overall performance of the material, we measured the p-type characteristics of the same devices, as shown in Figure S4 (Supporting Information). In contrast to the n-type performance, in the case of the p-type devices, the pristine DPP-T-TT device shows higher hole current compared to that measured for the device with the PEG interlayer. Furthermore, introducing the PEG interlayer led to an increase of the p-type turn-on voltage from −6 to −12 V (at V_{Drain} = −20 V) indicating that the PEG interlayer increased the hole injection barrier compared to the pristine device.

To understand the effect of the PEG interlayer on the interfacial energy level alignment, we fabricated an OFET with a Ca/Al contact and compared its n-type performance to that of the OFETs with Al or PEG/Al contacts. The work function of Ca is 2.88 eV,[32] sufficiently lower than the LUMO level of DPP-T-TT effectively allowing Fermi-level pinning and barrier-less electron injection.[33] The output characteristics of the Ca/Al device, Figure 2c, is similar to that of the OFET with the PEG interlayer, Figure 2b, with a similar overall current level and a linear increase of drain-current at a low drain-source voltage (insets). The V_{th} and corresponding saturation electron mobility of the Ca/Al device are 8.8 V and 0.16 cm^2 V^{-1} s^{-1}, respectively, which are also comparable to those of the PEG/Al contact device. The similarities between

DOI: 10.1021/acs.chemmater.9b01787
Chem. Mater. XXXX, XXX, XXX−XXX

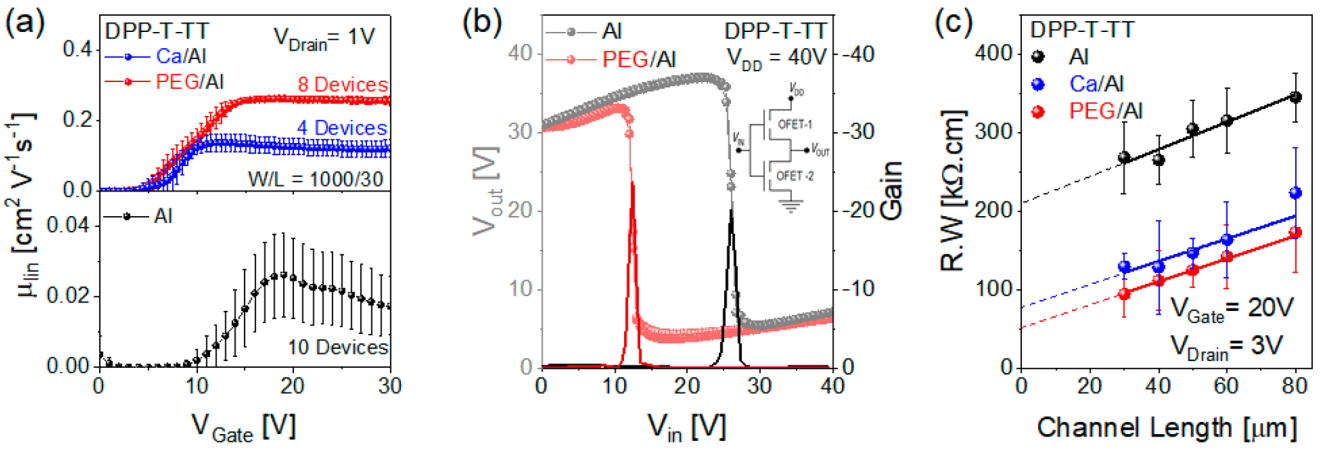

Figure 3. (a) Comparison of linear region field-effect mobility as a function of V_{Gate}, measured from transconductance for the OFETs biased at V_{Drain} of 1 V, including the statistical yield. (b) The transfer characteristics and gain of a complementary-like inverter comprised of two identical OFETs (L = 30 μm and W = 1000 μm) with and without PEG additive (inset: inverter circuit configuration). (c) TLM: width-normalized total resistance as a function of channel lengths to compare the contact resistance of the OFETs at V_{Gate} = 20 V.

these devices suggests that the self-generated PEG interlayer eliminates the barrier for electron injection. We speculate that the PEG molecules induce a dipole effect that modifies the EWF at the DPP-T-TT/Al interface that aligns the energy levels between the LUMO of the polymer and the metal work function, as illustrated in Figure 2e (right panel). Therefore, introducing the PEG interlayer both limits the direct pinning of the Al electrode to the DPP-T-TT[28] and also imposes a dipole-induced energy-level alignment that augments contact "selectively" toward electrons.

For further comparison, we calculated the differential linear-region field-effect mobility as a function of gate-source voltage (using Equation S2, Supporting Information) for OFET devices with and without PEG, as shown in Figure 3a. The linear mobility of the pristine device with Al contact (black line) initially increases and then decreases with increasing gate voltage. This type of gate voltage dependence has been previously associated with contact resistance modulation.[34] In contrast, for the devices with the PEG interlayer or Ca/Al contact (red and blue lines, respectively), the linear mobility value is constant irrespective of gate voltage. However, the device with the PEG interlayer shows higher linear mobility compared to that of the Ca/Al device, which is reflected in a steeper slope of the linear region drain current (see Figure S3 in the Supporting Information). The linear-region field-effect mobility is sensitive to contact resistance,[35] and therefore, the higher linear mobility of the device with the PEG interlayer could indicate lower contact resistance. The linear-region field-effect mobility is sensitive to contact resistance,[35] and therefore, the higher linear mobility of the device with the PEG interlayer could indicate lower contact resistance perhaps due to PEG-induced enhancement of polymer crystallinity at the organic/metal interface.

We qualitatively analyze the contribution of the PEG interlayer to the selectivity of the contact by comparing two inverters, one composed of two DPP-T-TT OFETs with Al contacts and the other composed of two DPP-T-TT OFETs with PEG/Al contacts. The voltage-transfer characteristics (output voltage, V_{out}, as a function of input voltage, V_{in}, for supply bias V_{DD} = 40 V) and corresponding gain of both inverters are shown in Figure 3b. All devices showed high stability over 10 continuous scans, as shown in Figure S5 (Supporting Information). Because of the p-type character of the D−A polymer, the inversion voltage of the inverter with Al contacts (black line) shifts to higher voltages compared to the ideal switching point at 1/2 V_{DD}. In contrast, the inversion voltage of the inverter with PEG/Al contacts (red line) shifts to lower voltages than the ideal switching point at 1/2 V_{DD}. This distinct negative shift suggests favorable n-channel operation due to higher electron concentration in the inverter confirming facile injection of electrons into the device.

For quantitative analysis of the effect of the PEG interlayer on EWF modulation, we performed TLM analysis to extract the contact resistance and channel resistance of all types of devices. Figure 3b shows the width-normalized device resistance ($R{\cdot}W$ for W = 1000 μm) of the DPP-T-TT OFETs without or with the PEG interlayer, with respect to the channel lengths (30, 40, 50, and 80 μm) at a gate-source voltage of 20 V. The width-normalized contact resistances and the channel resistances, extracted from the y-intercept and the slope of the least-squares linear fit of measured width-normalized device resistance, respectively, are listed in Table T1 (Supporting Information). One can easily notice that the contact resistance values (y-intercept) of the devices with a PEG interlayer or Ca/Al contact are comparable and almost four times lower than that of the pristine device with the Al contact. In contrast, the sheet resistance (figure slope) is similar in all devices confirming that although the PEG molecules are initially blended into the polymer solution, they do not affect the bulk active layer but rather the organic/contact interface.

In addition to the EWF and electronic properties, the generation of the PEG interlayer can also affect the molecular nanomorphology of the organic film and the organic/contact interface. Because of the abrupt decay of PEG content with respect to electrode distance, its effect on bulk and surface molecular order can significantly differ. Therefore, the comparison between PEG-induced surface and bulk nanomorphologies is extremely important to separately understand the contribution of PEG to contact resistance reduction, and channel conductivity enhancement. To shed light on the effect of PEG on the molecular packing at the DPPT-TT/Al interface compared to its effect on the bulk order, we performed GIWAXS experiments.[36] In contrast to most

DOI: 10.1021/acs.chemmater.9b01787
Chem. Mater. XXXX, XXX, XXX−XXX

GIWAXS measurements on organic electronic films, in this case we perform the measurements after depositing the metal contact. In the case of the self-generated interlayer, this is absolutely necessary because the contact generates the interlayer.

However, it is also worth mentioning that contact deposition could have an important impact on the interfacial nanomorphology and hence characterizing bare organic surfaces might not reflect the actual interfacial nanomorphology in the operational device. Generally, surface and bulk sensitivity are achieved by selection of incident angles below and above the typical critical angle (about 0.11°) of the organic film, respectively. Accordingly, using two different incident beam angles, 0.08° and 0.18°, allows us to compare the effect of PEG on scattering from the surface and the bulk of the film. Figure 4a,b show the GIWAXS patterns of DPP-T-TT and DPP-T-TT:PEG films with evaporated Al contacts acquired at the bulk-sensitive incident angle of 0.18°. In both patterns, we can identify first- and second-order peaks at Qz = 0.315 A^{-1} and at Qz = 0.62 A^{-1}, respectively, associated with DPP-T-TT polymer lamellar stacking (alkyl chains periodicity). The corresponding lamellar *d*-spacing is 19.9 Å, in good agreement with previous studies.[23,37] Figure 4c,d present GIWAXS patterns of the same DPP-T-TT and DPP-T-TT:PEG films collected strictly from the organic/Al interfaces by using an incident angle below the critical angle of the film (0.08°). The pristine DPP-T-TT pattern (Figure 4c) shows the same first- and second-order lamellar stacking peaks (Qz = 0.315 $Å^{-1}$ and Qz = 0.62 $Å^{-1}$, respectively) as in the bulk. The DPP-T-TT:PEG pattern (Figure 4d), on the other hand, shows significantly more intense lamellar stacking peaks, visible up to fourth order, indicating a substantial enhancement in polymer lamellar packing at the interface. The lamellar stacking peaks arise only along the Qz axis, for both bulk and surface, indicating an edge-on orientation of the backbone relative to the substrate (h00). The broad halo ring around Q = 1.5 A^{-1} which is seen in the bulk patterns (Figure 4a,b) arises from scattering due to amorphous regions in the film. Interestingly, the ratio of intensity of amorphous scattering to lamellar peak scattering is significantly lower in surface-sensitive measurements than in bulk measurements for all films suggesting a generally higher degree of order at the top surface compared to the bulk.

Formation of the PEG interlayer reduces the lamellar stacking peak area in the bulk by 20%, which is within expected experimental error (Figure 5a). In contrast, presence of the

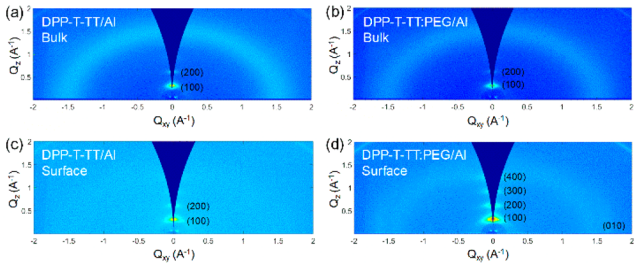

Figure 4. GIWAXS pattern of (a) bulk DPP-T-TT/Al and (b) bulk DPP-T-TT:PEG/Al acquired using an incident angle higher than the critical angle of the film (0.18°); (c) surface DPP-T-TT/Al and (d) surface DPP-T-TT:PEG/Al acquired using an incident angle lower than the critical angle of the film (0.08°).

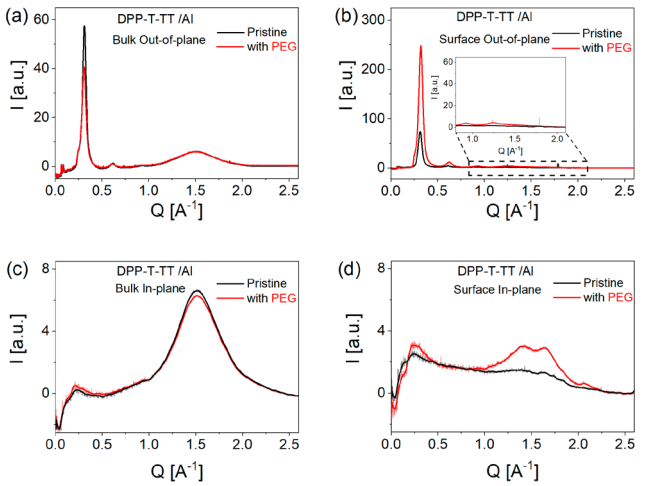

Figure 5. Reduced normalized integrated 1D spectra of DPP-T-TT with and without PEG for out-of-plane ($0° < \chi < 20°$) orientation: (a) bulk (0.18°), and (b) surface (0.08°) sensitive measurements (b-inset: magnification of amorphous scattering peak region); and for in-plane ($70° < \chi < 90°$) orientation: (c) bulk (0.18°), and (d) surface (0.08°) sensitive measurements.

PEG interlayer at the interface results in an incredible ~240% increase of the lamellar stacking peak area at the interface (Figure 5b). A $\pi-\pi$ stacking peak at Q ≈ 1.7 $Å^{-1}$ also becomes prominent in the in-plane direction (Figure 5d). Thus, PEG induces an increase in DPP-T-TT crystallinity at the interface while the bulk is virtually unchanged. The amorphous scattering peak (Q = 1.5 A^{-1}) area captured in the bulk remains unaffected by PEG presence for both out-of-plane (Figure 5a) and in-plane (Figure 5c) orientations. However, due to the reduction of lamellar peak area, the ratio of amorphous to lamellar peak intensity increases with PEG by ~20% (see Table T2). At the interface, however, amorphous scattering is reduced to an undetectable level for out-of-plane orientation (see inset in Figure 5b), while for the in-plane orientation, the amorphous scattering signal is enhanced with PEG.

The overall morphology characterization of DPP-T-TT and DPP-T-TT:PEG bulk do not demonstrate any obvious alteration of morphology associated with PEG incorporation. In contrast, the incredible enhancement of molecular order at the DPP-T-TT/Al interface, induced by PEG migration toward the metal contact, supports the n-type performance augmentation. Correlation between high n-type mobility and increased lamellar order of the bulk in the out-of-plane direction (usually obtained by thermal treatments or solvent additives) is well documented for the DPP-T-TT polymer.[23,37] Therefore, we hypothesize that the interfacial molecular order plays a massive role in reducing the electron injection barrier and consequently reduces the bulk-access resistance component of the overall contact resistance.

Finally, to show the versatility of the interlayer generation methodology for augmenting n-type performance in OFETs, we fabricated devices on flexible polyimide substrates with an Al_2O_3/CPVP dielectric layer. The Al_2O_3/CPVP dielectric layer exhibits lower electron trapping compared to a SiO_2 dielectric layer and is therefore more suitable for demonstrating n-type performance.[38−40] Figure 6a shows a schematic illustration of the device architecture (bottom) and an optical image of an array of 20 OFETs on the flexible substrate (top). In Figure 6b

DOI: 10.1021/acs.chemmater.9b01787
Chem. Mater. XXXX, XXX, XXX−XXX

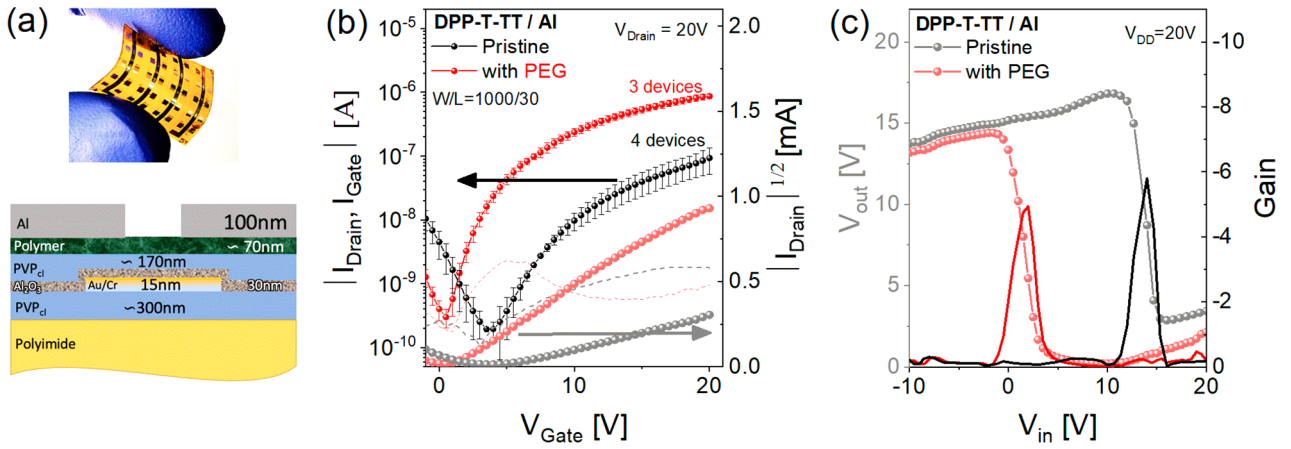

Figure 6. Flexible device architecture and characterization. (a) Top: optical image of flexible substrate with 20 OFET devices; bottom: the schematic of device architecture with dimensions. (b) Device performance comparison of flexible OFETs with and without PEG additive including the statistical yield. (c) The transfer characteristics and gain of a complementary-like-inverter composed of two identical OFETs (L = 30 μm and W = 1000 μm) with (red) and without (black) PEG additive.

we compare the performances of flexible OFETs with and without a PEG interlayer. The V_{th} of the flexible device with Al source-drain electrodes (i.e, no PEG interlayer) is ~5.0 V, while that with a generated PEG interlayer at the Al source-drain electrodes is ~0.7 ± 0.2 V. This significant reduction of V_{th} is similar to our previous observations of the OFETs on conventional silicon substrates (Figure 2) and indicates that the generated interlayer methodology is also suitable for the fabrication and processing of flexible devices. Furthermore, comparing the performance of inverters fabricated on the flexible substrate with and without the PEG interlayers, Figure 6c, shows again that the PEG interlayer shifts the inversion voltage to lower values relative to the reference device (no PEG interlayer) and ideal switching point (1/2 V_{DD}). This result shows unambiguously that the PEG interlayer facilities electron injection allowing high electron concentration, effectively inducing favorable n-channel operation.

SUMMARY AND CONCLUSIONS

In summary, using DPP-T-TT OFETs as a platform, we showed that n-type performance of D−A polymer can be significantly enhanced when PEG additive molecules are blended into the polymer solution. Strong affinity between the hydroxyl end-groups of PEG and the top Al contact induces PEG migration to the polymer/metal interface during Al deposition to form an interlayer. XPS measurements confirm presence of the interlayer at the interface while GIWAXS measurements indicate that generation of the interlayer induces a significant increase in the lamellar ordering of the polymer at the interface. The effect of the self-generated PEG interlayer and the induced polymer ordering on the electrical performance of the n-type OFETs was investigated in terms of the electron field-effect mobility (μ_{FET}), turn-on and threshold voltage (V_{ON} and V_{th}), inverter performance and contact resistance (R_C). We find that the self-generated PEG interlayer has a dual role: first, it modifies the EWF at the buried metal/organic interface, making the contact selective for electron injection; and second, it induces molecular ordering at the interface that supports electron transport, effectively reducing the bulk-access resistance. This methodology to augment n-type performance of an ambipolar polymer OFET on flexible substrates by self-generated interlayers is compatible with printing and R2R processing and can therefore be integrated into high-throughput fabrication processes.

EXPERIMENTAL SECTION

Materials. DPP-T-TT (Mw = 30 000 g mol $^{-1}$, PDI = 3) was purchased from Ossila Limited. PEG (Mw = 200 g mol^{-1}), trichloro(octadecyl)silane (Mw = 387.93 g mol $^{-1}$), poly-4-vinyl-phenol (PVP) (Mw = 25 000 g mol $^{-1}$), poly(melamine-*co*-formaldehyde) methylated (MMF) (M_n ~ 432, 84 wt % in 1-butanol), and propylene glycol monomethyl ether acetate (PGMEA) were purchased from Sigma-Aldrich. All materials were used as received. Silicon substrates with 220 nm SiO_2 layer were purchased from University Wafer Inc.

Device Fabrication. Heavily p-doped silicon wafers with a 200 nm SiO_2 dielectric layer were used as substrates. Si-substrates were cleaned by sonication in acetone for 5 min and then immersed in piranha solution for 20 min at 100C and several times in distilled water. Finally, substrates were washed by 2-propanol for 10 min in sonication. The cleaned substrates were treated by trichloro-(octadecyl) silane (OTS) in a vacuum oven at 90C for 30 min. OTS-treated substrates were cleaned two times in toluene and one time in 2-propanol, separately, for 5 min each and dried by nitrogen. 1,2-Dichlorobenzene solutions of DPP-T- TT (7 mg/mL), PEG (10 mg/mL) were prepared and mixed to obtain solutions of DPP-T-TT:PEG 5:0 mg/mL (reference) and 5:0.5 mg/mL. All active semiconducting layers were deposited by spin-coating polymer solution at 2000 rpm for 140 s. The spin-coated films were dried overnight in nitrogen condition in room temperature. Finally, 100 nm-thick aluminum electrodes were deposited through a shadow mask, using a thermal evaporator at a deposition rate of 2 Å s^{-1} under 5 × 10 $^{-6}$ Torr at room temperature for the source/drain electrodes of the OFETs.

For the flexible device, a 300 nm planarizing layer of cross-linkable PVP (12%) and MMF (6%) solution in PGMEA was spin coated on the flexible polyimide substrates after cleaning with acetone, ethanol, and deionized water. The PVP layer was cross-linked at 180 °C in vacuum oven for 1 h. On the cross-linked PVP layer, 15 nm chromium/gold gate electrode was deposited through the shadow masks. In the next step, a 30 nm alumina dialectic layer was deposited using the ALD technique followed by the deposition of 150 nm cross-linkable PVP dielectric layer through the spin coating. After cross-linking the PVP dielectric layer, the active layer (with or without PEG) and the 100 nm thick source-drain electrodes were deposited in same way as discussed above.

Grazing-Incidence Wide-Angle X-ray Scattering (GIWAXS). Grazing-incidence wide-angle X-ray scattering was measured at the Stanford Synchrotron Radiation Lightsource (SSRL) beamline 11-3 in

DOI: 10.1021/acs.chemmater.9b01787
Chem. Mater. XXXX, XXX, XXX−XXX

a helium-filled chamber with an X-ray wavelength of 0.9752 Å and sample-to-detector distance of 25 cm at an incident angle of 0.18° and 0.08° for bulk and surface sensitive modes, respectively. The incident angle for bulk measurements is well above the critical angle of the thin film and the silicon substrate, while the surface-sensitive angle is well below the critical angle of the film. These angles were selected away from the film critical angle (~0.11°) to reduce the effect of slight errors in incident angle on the scattering intensity. The spectra were collected by a 2D X-ray detector (MX225, Rayonix, L.L.C) with a pixel size of 73 μm (3072 × 3072 pixels) and analyzed using the Nika package for Wavemetrics Igor software in combination with WAXS tools.[41,42] The length and thickness of the measured samples were kept constant, and the reduced 1-D spectra were normalized by the intensity of incident beam.

X-ray Photoelectron Spectroscopy (XPS). X-ray photoelectron spectroscopy measurements were performed in an analysis chamber (UHV − 210^{-10} Torr during analysis) using a Versaprobe III − PHI Instrument (PHI, U.S.A.). The sample was irradiated with a focused X-ray Al Kα monochromatic X-ray source (1486.6 eV) using (X-ray beam size diameter: 200 μm, 25W, 15KV). The outgoing photoelectrons were directed to a Spherical Capacitor neutralization Analyzer (SCA). The sample charging was compensated by dual beam charge neutralization based on a combination of a traditional electron flood gun and a low energy argon ion beam. The core level binding energies scans of C 1s were obtained with energy pass of 55 eV and recorded with an angle of 45° ± 3°. Based on the inelastic mean free path estimation of the metal/blend system, the information depth of the C 1s electrons is ~4 nm thick organic film beneath the aluminum layer. Line shape analysis was done using the XPSPEAK 4.1 software after Shirley-type background subtraction.

Device Characterization. Device characterization was performed inside a nitrogen-filled glovebox atmosphere under dark condition using an Agilent B1500-A semiconductor parameter analyzer and Keithley 2612B dual source-meter.

■ ASSOCIATED CONTENT

Supporting Information

The Supporting Information is available free of charge on the ACS Publications website at DOI: 10.1021/acs.chemmater.9b01787.

UV−vis absorption spectra, XPS characterization, calculation details, comparison of OFET characteristics, and extracted parameters of device performance and GIWAXS (PDF)

■ AUTHOR INFORMATION

Corresponding Author

*E-mail: gitti@technion.ac.il.

ORCID

Michael F. Toney: 0000-0002-7513-1166

Gitti L. Frey: 0000-0002-7638-4712

Notes

The authors declare no competing financial interest.

■ ACKNOWLEDGMENTS

The authors thank Prof. Nir Tessler from the Electrical Engineering Department of the Technion for helpful discussions. T.S. and G.F. are grateful for support by the Marie Skłodowska-Curie Actions Innovative Training Network "H2020-MSCAITN-2014 INFORM − 675867". This work was also supported by the Office of Naval Research NDSEG fellowship (to V.S.). Work was partially supported by the Department of the Navy, Office of Naval Research Award No. N00014-14-1-0580 (to M.F.T.). Use of the Stanford Synchrotron Radiation Lightsource, SLAC National Accelerator Laboratory, is supported by the U.S. Department of Energy, Office of Science, Office of Basic Energy Sciences under Contract No. DE-AC02-76SF00515.

■ REFERENCES

(1) Lai, S.; Casula, G.; Cosseddu, P.; Basiricò, L.; Ciavatti, A.; D'Annunzio, F.; Loussert, C.; Fischer, V.; Fraboni, B.; Barbaro, M.; Bonfiglio, A. A plastic electronic circuit based on low voltage, organic thin-film transistors for monitoring the X-Ray checking history of luggage in airports. *Org. Electron.* **2018**, *58*, 263−269.

(2) Viola, F. A.; Spanu, A.; Ricci, P. C.; Bonfiglio, A.; Cosseddu, P. Ultrathin, flexible and multimodal tactile sensors based on organic field-effect transistors. *Sci. Rep.* **2018**, *8* (1), 8073.

(3) She, X.-J.; Gustafsson, D.; Sirringhaus, H. A Vertical Organic Transistor Architecture for Fast Nonvolatile Memory. *Adv. Mater.* **2017**, *29* (8), 1604769.

(4) Ullah, M.; Wawrzinek, R.; Maasoumi, F.; Lo, S.-C.; Namdas, E. B. Semitransparent and Low-Voltage Operating Organic Light-Emitting Field-Effect Transistors Processed at Low Temperatures. *Adv. Opt. Mater.* **2016**, *4* (7), 1022−1026.

(5) Song, J.; Dailey, J.; Li, H.; Jang, H.-J.; Russell, L.; Zhang, P.; Searson, P. C.; Wang, J. T.-H.; Everett, A. D.; Katz, H. E. Influence of Bioreceptor Layer Structure on Myelin Basic Protein Detection using Organic Field Effect Transistor-Based Biosensors. *Adv. Funct. Mater.* **2018**, *28* (37), 1802605.

(6) Li, J.; Zhao, Y.; Tan, H. S.; Guo, Y.; Di, C.-A.; Yu, G.; Liu, Y.; Lin, M.; Lim, S. H.; Zhou, Y.; Su, H.; Ong, B. S. A stable solution-processed polymer semiconductor with record high-mobility for printed transistors. *Sci. Rep.* **2012**, *2*, 754.

(7) Sun, B.; Hong, W.; Yan, Z.; Aziz, H.; Li, Y. Record High Electron Mobility of 6.3 cm2V−1s−1 Achieved for Polymer Semiconductors Using a New Building Block. *Adv. Mater.* **2014**, *26* (17), 2636−2642.

(8) Kang, I.; Yun, H.-J.; Chung, D. S.; Kwon, S.-K.; Kim, Y.-H. Record High Hole Mobility in Polymer Semiconductors via Side-Chain Engineering. *J. Am. Chem. Soc.* **2013**, *135* (40), 14896−14899.

(9) Luo, H.; Yu, C.; Liu, Z.; Zhang, G.; Geng, H.; Yi, Y.; Broch, K.; Hu, Y.; Sadhanala, A.; Jiang, L.; Qi, P.; Cai, Z.; Sirringhaus, H.; Zhang, D. Remarkable enhancement of charge carrier mobility of conjugated polymer field-effect transistors upon incorporating an ionic additive. *Science Advances* **2016**, *2* (5), No. e1600076.

(10) Yan, H.; Chen, Z.; Zheng, Y.; Newman, C.; Quinn, J. R.; Dötz, F.; Kastler, M.; Facchetti, A. A high-mobility electron-transporting polymer for printed transistors. *Nature* **2009**, *457*, 679.

(11) Sun, B.; Hong, W.; Thibau, E. S.; Aziz, H.; Lu, Z.-H.; Li, Y. Polyethylenimine (PEI) As an Effective Dopant To Conveniently Convert Ambipolar and p-Type Polymers into Unipolar n-Type Polymers. *ACS Appl. Mater. Interfaces* **2015**, *7* (33), 18662−18671.

(12) Xu, Y.; Sun, H.; Li, W.; Lin, Y.-F.; Balestra, F.; Ghibaudo, G.; Noh, Y.-Y. Exploring the Charge Transport in Conjugated Polymers. *Adv. Mater.* **2017**, *29* (41), 1702729.

(13) Kano, M.; Minari, T.; Tsukagoshi, K. Improvement of subthreshold current transport by contact interface modification in p-type organic field-effect transistors. *Appl. Phys. Lett.* **2009**, *94* (14), 143304.

(14) Cheng, X.; Noh, Y.-Y.; Wang, J.; Tello, M.; Frisch, J.; Blum, R.-P.; Vollmer, A.; Rabe, J. P.; Koch, N.; Sirringhaus, H. Controlling Electron and Hole Charge Injection in Ambipolar Organic Field-Effect Transistors by Self-Assembled Monolayers. *Adv. Funct. Mater.* **2009**, *19* (15), 2407−2415.

(15) Ito, Y.; Virkar, A. A.; Mannsfeld, S.; Oh, J. H.; Toney, M.; Locklin, J.; Bao, Z. Crystalline Ultrasmooth Self-Assembled Monolayers of Alkylsilanes for Organic Field-Effect Transistors. *J. Am. Chem. Soc.* **2009**, *131* (26), 9396−9404.

(16) Roh, J.; Lee, T.; Kang, C.-m.; Kwak, J.; Lang, P.; Horowitz, G.; Kim, H.; Lee, C. Injection-modulated polarity conversion by charge carrier density control via a self-assembled monolayer for all-solution-processed organic field-effect transistors. *Sci. Rep.* **2017**, *7*, 46365.

DOI: 10.1021/acs.chemmater.9b01787
Chem. Mater. XXXX, XXX, XXX−XXX

(17) Hong, J.-P.; Park, A.-Y.; Lee, S.; Kang, J.; Shin, N.; Yoon, D. Y. Tuning of Ag work functions by self-assembled monolayers of aromatic thiols for an efficient hole injection for solution processed triisopropylsilylethynyl pentacene organic thin film transistors. *Appl. Phys. Lett.* **2008**, *92* (14), 143311.
(18) Sarkar, T.; Shamieh, B.; Verbeek, R.; Kronemeijer, A. J.; Gelinck, G. H.; Frey, G. L. Tuning Contact Resistance in Top-Contact p-Type and n-Type Organic Field Effect Transistors by Self-Generated Interlayers. *Adv. Funct. Mater.* **2019**, *0* (0), 1805617.
(19) Vinokur, J.; Deckman, I.; Sarkar, T.; Nouzman, L.; Shamieh, B.; Frey, G. L. Interlayers Self-Generated by Additive−Metal Interactions in Organic Electronic Devices. *Adv. Mater.* **2018**, *30* (41), 1706803.
(20) Kolesov, V. A.; Fuentes-Hernandez, C.; Chou, W.-F.; Aizawa, N.; Larrain, F. A.; Wang, M.; Perrotta, A.; Choi, S.; Graham, S.; Bazan, G. C.; Nguyen, T.-Q.; Marder, S. R.; Kippelen, B. Solution-based electrical doping of semiconducting polymer films over a limited depth. *Nat. Mater.* **2017**, *16*, 474.
(21) Li, L.; Xiao, L.; Qin, H.; Gao, K.; Peng, J.; Cao, Y.; Liu, F.; Russell, T. P.; Peng, X. High-Efficiency Small Molecule-Based Bulk-Heterojunction Solar Cells Enhanced by Additive Annealing. *ACS Appl. Mater. Interfaces* **2015**, *7* (38), 21495−21502.
(22) Razzell-Hollis, J.; Tsoi, W. C.; Kim, J.-S. Directly probing the molecular order of conjugated polymer in OPV blends induced by different film thicknesses, substrates and additives. *J. Mater. Chem. C* **2013**, *1* (39), 6235−6243.
(23) Chen, Z.; Lee, M. J.; Shahid Ashraf, R.; Gu, Y.; Albert-Seifried, S.; Meedom Nielsen, M.; Schroeder, B.; Anthopoulos, T. D.; Heeney, M.; McCulloch, I.; Sirringhaus, H. High-Performance Ambipolar Diketopyrrolopyrrole-Thieno[3,2-b]thiophene Copolymer Field-Effect Transistors with Balanced Hole and Electron Mobilities. *Adv. Mater.* **2012**, *24* (5), 647−652.
(24) Jeng, J.-Y.; Lin, M.-W.; Hsu, Y.-J.; Wen, T.-C.; Guo, T.-F. The Roles of Poly(Ethylene Oxide) Electrode Buffers in Efficient Polymer Photovoltaics. *Adv. Energy Mater.* **2011**, *1* (6), 1192−1198.
(25) Dekman, I.; Brener, R.; Frey, G. L. Thermal metal deposition induces segregation in polymer thin films: a demonstration on OPVs. *J. Mater. Chem. C* **2013**, *1* (40), 6522−6525.
(26) Fisher, G. L.; Walker, A. V.; Hooper, A. E.; Tighe, T. B.; Bahnck, K. B.; Skriba, H. T.; Reinard, M. D.; Haynie, B. C.; Opila, R. L.; Winograd, N.; Allara, D. L. Bond Insertion, Complexation, and Penetration Pathways of Vapor-Deposited Aluminum Atoms with HO- and CH3O-Terminated Organic Monolayers. *J. Am. Chem. Soc.* **2002**, *124* (19), 5528−5541.
(27) Li, W.; Hendriks, K. H.; Roelofs, W. S. C.; Kim, Y.; Wienk, M. M.; Janssen, R. A. J. Efficient Small Bandgap Polymer Solar Cells with High Fill Factors for 300 nm Thick Films. *Adv. Mater.* **2013**, *25* (23), 3182−3186.
(28) Magen, O.; Tessler, N. On electrode pinning and charge blocking layers in organic solar cells. *J. Appl. Phys.* **2017**, *121* (19), 195502.
(29) Connelly, D.; Faulkner, C.; Clifton, P. A.; Grupp, D. E. Fermi-level depinning for low-barrier Schottky source/drain transistors. *Appl. Phys. Lett.* **2006**, *88* (1), 012105.
(30) Xu, J.; Wang, S.; Wang, G.-J. N.; Zhu, C.; Luo, S.; Jin, L.; Gu, X.; Chen, S.; Feig, V. R.; To, J. W. F.; Rondeau-Gagné, S.; Park, J.; Schroeder, B. C.; Lu, C.; Oh, J. Y.; Wang, Y.; Kim, Y.-H.; Yan, H.; Sinclair, R.; Zhou, D.; Xue, G.; Murmann, B.; Linder, C.; Cai, W.; Tok, J. B. H.; Chung, J. W.; Bao, Z. Highly stretchable polymer semiconductor films through the nanoconfinement effect. *Science* **2017**, *355* (6320), 59.
(31) Uglea, C. V. *Oligomer Technology and Applications*, 1st ed.; CRC Press: Boca Raton, FL, 1998; pp 249−298.
(32) Michaelson, H. B. The work function of the elements and its periodicity. *J. Appl. Phys.* **1977**, *48* (11), 4729−4733.
(33) Braun, S.; Salaneck, W. R.; Fahlman, M. Energy-Level Alignment at Organic/Metal and Organic/Organic Interfaces. *Adv. Mater.* **2009**, *21* (14−15), 1450−1472.
(34) Bittle, E. G.; Basham, J. I.; Jackson, T. N.; Jurchescu, O. D.; Gundlach, D. J. Mobility overestimation due to gated contacts in organic field-effect transistors. *Nat. Commun.* **2016**, *7*, 10908.
(35) Fortunato, E.; Barquinha, P.; Martins, R. Oxide Semiconductor Thin-Film Transistors: A Review of Recent Advances. *Adv. Mater.* **2012**, *24* (22), 2945−2986.
(36) Rivnay, J.; Mannsfeld, S. C. B.; Miller, C. E.; Salleo, A.; Toney, M. F. Quantitative Determination of Organic Semiconductor Microstructure from the Molecular to Device Scale. *Chem. Rev.* **2012**, *112* (10), 5488−5519.
(37) Zhang, X.; Richter, L. J.; DeLongchamp, D. M.; Kline, R. J.; Hammond, M. R.; McCulloch, I.; Heeney, M.; Ashraf, R. S.; Smith, J. N.; Anthopoulos, T. D.; Schroeder, B.; Geerts, Y. H.; Fischer, D. A.; Toney, M. F. Molecular Packing of High-Mobility Diketo Pyrrolo-Pyrrole Polymer Semiconductors with Branched Alkyl Side Chains. *J. Am. Chem. Soc.* **2011**, *133* (38), 15073−15084.
(38) Mathijssen, S. G. J.; Kemerink, M.; Sharma, A.; Cölle, M.; Bobbert, P. A.; Janssen, R. A. J.; de Leeuw, D. M. Charge Trapping at the Dielectric of Organic Transistors Visualized in Real Time and Space. *Adv. Mater.* **2008**, *20* (5), 975−979.
(39) Chua, L.-L.; Zaumseil, J.; Chang, J.-F.; Ou, E. C. W.; Ho, P. K. H.; Sirringhaus, H.; Friend, R. H. General observation of n-type field-effect behaviour in organic semiconductors. *Nature* **2005**, *434* (7030), 194−199.
(40) Yoon, M.-H.; Yan, H.; Facchetti, A.; Marks, T. J. Low-Voltage Organic Field-Effect Transistors and Inverters Enabled by Ultrathin Cross-Linked Polymers as Gate Dielectrics. *J. Am. Chem. Soc.* **2005**, *127* (29), 10388−10395.
(41) Oosterhout, S. D.; Savikhin, V.; Zhang, J.; Zhang, Y.; Burgers, M. A.; Marder, S. R.; Bazan, G. C.; Toney, M. F. Mixing Behavior in Small Molecule:Fullerene Organic Photovoltaics. *Chem. Mater.* **2017**, *29* (7), 3062−3069.
(42) Ilavsky, J. Nika: software for two-dimensional data reduction. *J. Appl. Crystallogr.* **2012**, *45* (2), 324−328.

DOI: 10.1021/acs.chemmater.9b01787
Chem. Mater. XXXX, XXX, XXX−XXX